Publication III

Ari Poikonen and Seppo Madekivi. 2010. Wind-generated ambient noise in a shallow brackish water environment in the archipelago of the Gulf of Finland. The Journal of the Acoustical Society of America, volume 127, number 6, pages 3385-3393.

Wind-generated ambient noise in a shallow brackish water environment in the archipelago of the Gulf of Finland

Ari Poikonen[a] and Seppo Madekivi
Finnish Naval Research Institute, P.O. Box 116, FIN-02631 Espoo, Finland

(Received 10 September 2009; revised 30 January 2010; accepted 12 March 2010)

Underwater ambient noise measurements were carried out in a shallow (15–20 m) brackish water in the archipelago of the Gulf of Finland for period of 1 year. The absence of traffic noise made it possible to study wind driven effects in ambient noise at lower frequencies. The ambient noise comes mostly from local sources and the propagation effects are shown to be negligible. The ambient noise develops bubble type spectral features above 100 Hz as wind speed increases. Sharp spectral declines are observed below 500 Hz, which are most likely due to resonances from oscillating bubble clouds created by breaking waves. The low frequency range of the observed declines may partly be attributed to the larger bubble size in fresh and brackish waters. In the present study the wind speed dependence factor was ~2.4 at 200 Hz, which is significantly higher than the typical factor of ~1.5 for the ocean environment. The average high-frequency spectral slope was −4.9 dB/octave which is ~1 dB/octave less than for typical deep water slopes. No significant seasonal effects were found in any parameter calculated from the ambient noise spectra.
 [DOI: 10.1121/1.3397364]

PACS number(s): 43.30.Nb [WMC] Pages: 3385–3393

I. INTRODUCTION

Underwater ambient noise has been studied systematically since the 1940s. A comprehensive summary of the early deep water results was given by Wenz (1962), while fundamental ambient noise characteristics from studies prior to the early 1980s were reviewed by Urick (1984). Research activity on natural mechanisms and physical sources of ambient noise increased in the 1980s and breaking waves became the subject of intensive study (Kerman, 1984). A comprehensive review on low-frequency ambient noise was given by Carey and Browning (1988). By the early 1990s it was generally recognized that the major contributors to low-frequency underwater ambient noise are oscillating bubbles and bubble clouds generated by breaking waves. At higher frequencies combinations of bubble, spray, splash, and turbulence caused by breaking waves are primary sources of sound (Carey and Fitzgerald, 1993; Prosperetti, 1988; Yoon *et al.*, 1991). A persistent problem in the low-frequency studies, however, is the difficulty in acquiring ambient noise data below 500 Hz without the dominating influence of traffic noise.

It is well established that bubble size distribution in sea water is controlled by salinity although experimental results are quite variable depending on the method used. The effect of salinity on ambient noise caused by breaking waves was simulated with a tipping trough experiment by Carey *et al.* (1993). They showed that the salinity controls bubble size distribution such that the proportion of small bubbles increases markedly as salinity is raised. This was seen as higher ambient noise levels (NLs) above 4 kHz. The level of acoustic radiation was also found to depend on salinity. In another laboratory experiment breaking waves were simulated in a wave tank where the bubble size spectra were found to be ten times higher in oceanic-like saltwater than in fresh tap water (Su and Cartmill, 1995). Winkel *et al.* (2004) reported a study where air was injected into a flowing liquid with varying salinity. The mean bubble diameter dropped to one-quarter of that for fresh to brackish water (0–9 ppt) in 33 ppt saltwater. The resonance frequency of a bubble is inversely proportional to the bubble radius (Urick, 1983a) which therefore predicts that the resonance frequency of the saltwater bubbles in this experiment should be four times higher than that of the freshwater bubbles. This is perhaps not directly applicable to the breaking wave environment because the air injection itself may affect the bubble size distribution. The common trend in all the experiments is, however, the tendency of a bubble to grow in size as salinity decreases. This is because freshwater bubbles coalesce easily, whereas saltwater bubbles repel each other due to their different surficial physical-chemical properties (Su and Cartmill, 1995).

The present study deals with ambient noise measurements in shallow brackish water in an archipelago environment in the Gulf of Finland. Surface salinity in the Baltic Sea basin varies from 6 to 9 ppt and in the Gulf Finland it decreases from 6 ppt in the west to 3 ppt in the east (Kullenberg, 1981). The coastal waters of Finland and Sweden in the Baltic Sea are characterized by the abundance of islands which form confined water areas. These areas in the archipelago are typically shielded against low-frequency traffic noise from major sea lines.

Shallow water measurements have a tendency to be site dependent due to differences in sea bed properties, water depth, and propagation conditions (Ingenito and Wolf, 1989). On the other hand Urick (1984) noted that the poor transmission in shallow water allows locally generated wind noise to dominate the spectrum at all frequencies. We estimate the

[a]Author to whom correspondence should be addressed. Electronic mail: ari.poikonen@mil.fi.

propagation effects with a simple noise model which calculates the noise field from a surface dipole distribution in the presence of bottom sediment. The present ambient noise data set covers a full 1-year period, based on measurements made between August, 2006 and August, 2007. The wind conditions varied from calm sea up to near gale force winds. Measurements were also made in winter conditions where the sea was frozen. Ambient noise spectra are parametrized with a logarithmic model fitted to measured noise spectra. The ambient noise data are analyzed using the model parameters, and the results are compared to previous studies in oceanic areas.

II. PHYSICAL ENVIRONMENT AND EXPERIMENT DESCRIPTION

The measurement site is located in the archipelago of the western part of the Gulf of Finland and is isolated from the major sea lines by islands and shoals. The measurements were not corrupted by traffic noise which made it possible to study the wind driven effects on ambient noise at lower frequencies. The fetch of the wind at the site varies from a few kilometers up to several tens of kilometers depending on direction. The maximum significant wave height in the area during gale force winds was 0.5–1 m which corresponds to sea state 3 in the ocean environment. The average depth around the hydrophone is 15–20 m. Bottom sediments at the site are typically postglacial silt and clay. The salinity of the sea water at the site varies between 5 and 6 ppt. Temperature and sound speed profiles remained quite flat throughout the year because of strong mixing within this shallow archipelago environment. The water temperature varies from 0° in winter to around 20° in summer. These annual variations correspond to sound velocities ranging from 1410 to 1490 m/s, respectively. Meteorological sensors were set up at 10 m above sea level on the top of the station to provide temperature, pressure, and wind conditions during the measurements.

A calibrated omnidirectional hydrophone (TC4032) was deployed in a tripod on the sea bed at a depth of 16 m and about 500 m from the shore, Fig. 1(a). The hydrophone has a flat frequency response (2.5 dB) from 10 Hz to 80 kHz and a sensitivity of -170 dB re V/μPa. The hydrophone signal was transferred to the shore in analog form. The data acquisition system was built on high-quality consumer audio components. The analog signal from the preamplifier was sampled with 16-bit resolution in the external sound card at a standard audio sample rate of 44.1 kHz. The noise samples were stored in uncompressed audio format (wav) on hard disk for postprocessing.

Ambient noise samples with durations of several minutes were stored together with the meteorological data. Power spectral density (PSD) estimates for the samples were calculated using the periodogram with a rectangular window. The raw spectrum levels were obtained as the average of 32 1-s samples. Interfering frequency lines, such as power harmonics, were then removed from the spectra using the nonlinear nine-point median filtering. The final smoothing was performed by calculating total power for 1/3-octave bands and then normalizing the band power to a 1-Hz band.

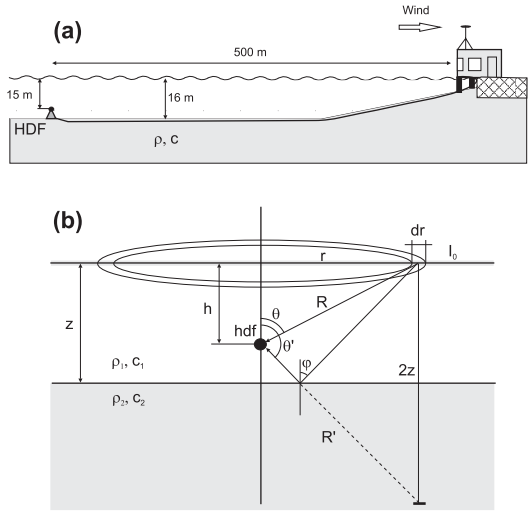

FIG. 1. (a) Experimental setup for measuring ambient noise in shallow water. (b) Geometry and notation of the noise model. ρ_i is the density and c_i is the sound velocity of the medium i.

III. MODEL DESCRIPTION

A. Physical noise model

Measured noise levels vary from site-to-site depending on the properties of the sea bottom. In order to estimate and remove the bottom effect a noise model is needed. Burgess and Kewley (1983) introduced a simple ocean model which was used to obtain surface source levels (SLs) from vertical linear array data. Kennedy and Szlyk (1991) showed by vertical directional measurements that the ambient noise field has a dipole characteristic when whitecaps are present in breaking waves. Lurton (2002) has presented a model for calculating the acoustic intensity from the infinite dipole distribution at the sea surface. If the absorption is negligible the relationship between noise level and source level in homogeneous deep water is given by $I_D = \pi I_0$, where I_0 is the average intensity per unit area created by the dipole distribution and I_D is the intensity of the noise field.

A "first-order" approximation of the bottom-reflected noise field can be calculated by the image method using only the first reflection, according to the geometry and notation shown in Fig. 1(b). The water column has constant sound velocity in order to keep the model simple. The intensity element of integration

$$dI_R = \frac{V^2(\varphi) 2\pi r dr I(\theta')}{R'^2} e^{-\beta R'}, \tag{1}$$

where $V^2(\varphi)$ is the plane wave reflection coefficient for intensity and $\beta = \alpha/4.343$ (α in dB/m) is the absorption coefficient for intensity. Using elementary trigonometry and completing the integral with respect to zenith angle θ, we get

$$I_R = 2\pi I_0 \int_0^{\pi/2} \frac{V^2(\varphi(\theta))\tan\ \theta f(\theta,z,h)}{g(\theta,z,h)} e^{-\beta R'} d\theta, \tag{2}$$

where

$$f(\theta,z,h) = \cos^2\ \theta' = \left[\frac{h^2(1-\tan^2\ \theta) + R'^2 - 4z^2}{2hR'}\right]^2,$$

$$g(\theta,z,h) = \left(\frac{R'}{R}\right)^2 = 1 + \frac{4z\ \cos^2\ \theta}{h^2}(z-h),$$

$$R' = \sqrt{\frac{h^2}{\cos^2\ \theta} + 4z(z-h)},$$

and

$$\varphi(\theta) = \arctan\left[\frac{h\ \tan\ \theta}{(2z-h)}\right].$$

The plane wave reflection coefficient for intensity may be written as

$$V^2(\varphi) = \frac{\rho_2 c_2\ \cos\ \varphi - \rho_1 c_1\ \cos\ \nu}{\rho_2 c_2\ \cos\ \varphi + \rho_1 c_1\ \cos\ \nu}, \tag{3}$$

where ρ_i and c_i are the density and the sound velocity of the layer i. ν is the angle of transmission and its cosine is obtained from Snell's law as

$$\cos\ \nu = \sqrt{1 - \left(\frac{c_2}{c_1}\right)^2 \sin^2\ \varphi}. \tag{4}$$

Total intensity $I_T = I_D + I_R$ is obtained by integrating numerically the integral in Eq. (2). The model can be used to estimate the extent of the surface area where most of the noise energy comes from. The model parameters representing the actual conditions are water depth $z=16$ m and hydrophone depth $h=15$ m. The bottom sediment is silt and clay with $\rho=1600$ kg/m^3 and $c=1600$ m/s. The absorption coefficient β is less than 10^{-5} at frequencies below 10 kHz so the effect of absorption is negligible in the present calculations. Figure 2(a) shows how the ambient noise level accumulates as the angle of integration expands. The half-power value (−3 dB) is reached at the zenith angle of about 49°. This means that half of the noise power comes from the circular surface area having a diameter roughly twice the depth of the hydrophone. For an infinite water depth the same result was originally given by Urick (1984). In this case the diameter of the half-power circle on the sea surface is about 35 m.

The bottom-reflected noise field was studied with several sediment types typical in the Baltic Sea area (Poikonen and Madekivi, 2005). In Fig. 2(b) the difference between NL and SL is plotted against the impedance contrast Z_2/Z_1 where $Z_i = \rho_i c_i$ is the characteristic acoustic impedance of the medium i. Realistic impedance contrasts between the water and the sediment vary from 1 to 10. The baseline "10 log π" indicates the directly transmitted intensity with no bottom reflection ($I_R=0$). The nine typical Baltic sediment classes are marked as numbered dots in the plot. The calculation demonstrates that thick layers of recent mud and postglacial clay behave as a poorly reflecting bottom ($Z_2/Z_1 < 1.3$) whose contribution to the ambient noise level is less than 0.2 dB. The harder silt and clay bottom at the measuring site increases the ambient noise level by 1 dB over the soft bottom.

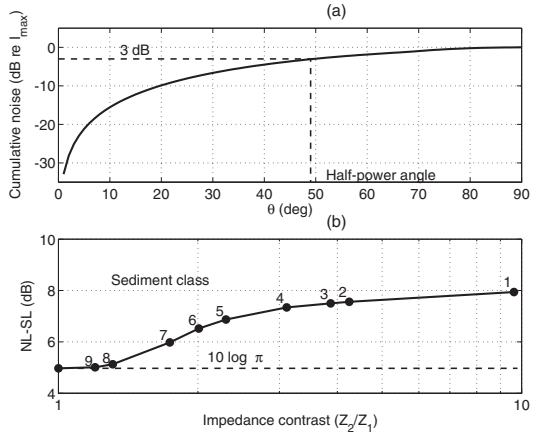

FIG. 2. (a) Accumulation of noise intensity with increasing zenith angle (θ). (b) Difference between NL and SL versus impedance contrast Z_2/Z_1 for nine typical Baltic sediment classes which are rock (1), till (2), till formation (3), sand and gravel (4), secondary sand (5), glacial mixture (6), silt and clay (7), postglacial clay (8), and recent mud (9).

B. Low-frequency sound propagation

Kuperman and Ferla (1985) calculated the acoustic field of wind-generated noise in a shallow water channel using two acoustic propagation models. The normal-mode solution gives propagating modes (discrete field) while the near field (continuous field) part is obtained with the fast-field program. They found that the continuous near field is virtually independent of frequency and the wind-induced noise remains essentially constant with depth.

Our model showed that half of the ambient noise power is generated within a cone with an aperture of about 100°, which means that the associated acoustic field is caused by local surface sources and is thus dominated by the near field solution. This leads to the conclusion that the frequency dependence of the ambient noise level measured on the bottom follows closely that of the source level on the surface. The discrete field from distant sources is subject to the low-frequency cutoff where the channel does not support propagating modes, leading to strong attenuation in sound level below the cutoff frequency. In a homogeneous water layer over a homogeneous bottom the cutoff frequency may be written as (Jensen *et al.*, 1994)

$$f_c = \frac{c_w}{4D\sqrt{1 - \left(\frac{c_w}{c_b}\right)^2}}, \tag{5}$$

where D is water depth, and c_w and c_b are sound speeds for the water and the bottom sediment, respectively. The cutoff frequencies for winter and summer conditions in the present

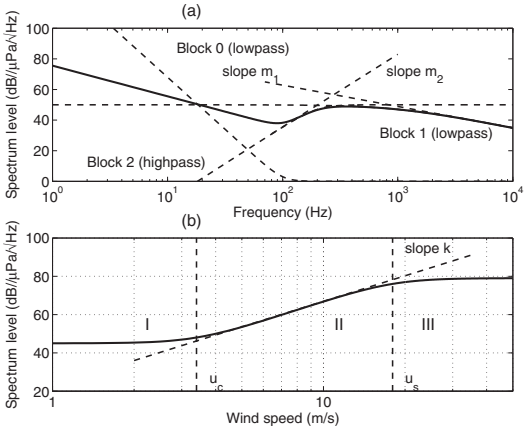

FIG. 3. (a) Logarithmic curve model for the parametrization of ambient noise spectrum. (b) Three wind speed regions in the ambient noise spectrum.

case are obtained from Eq. (5) using the actual parameters $D=16$ m, $c_b=1600$ m/s, and $c_w=1410-1490$ m/s. This results in two extremes for the cutoff frequency: 47 Hz for winter and 64 Hz for summer.

We conclude from the modeling that the effect of the sea bottom on ambient noise level is +1 dB, the total difference between NL and SL being about 6 dB. Due to the near field conditions the frequency dependence of the ambient noise level on the bottom is expected to conform with that of the ambient source level. If significant long-range propagation of acoustic energy existed there would a marked decrease in the spectrum level below the cutoff frequency (47–64 Hz).

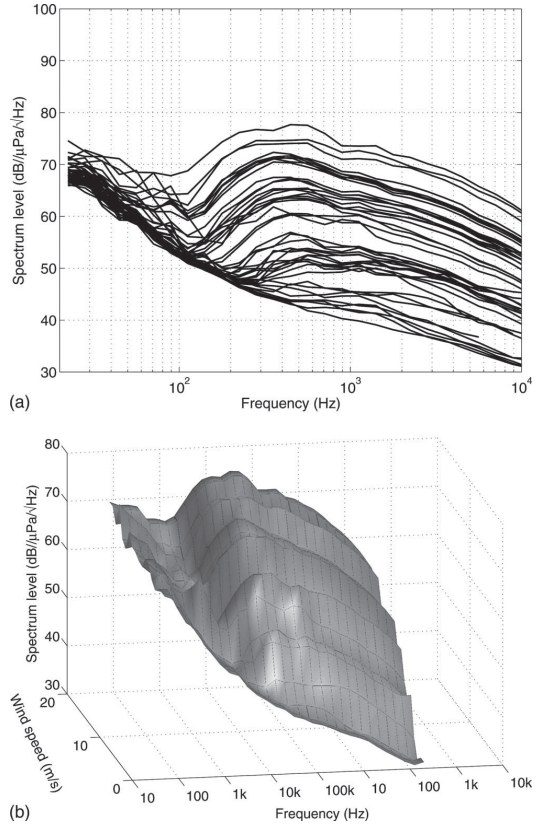

FIG. 4. (a) All of the measured spectra showing the range where the ambient noise varies as a function of wind speed. (b) The same data as a shaded surface: ambient noise as a function of frequency and wind speed.

C. Parametrization of measured spectra

1. Spectral parameters

Logarithmic expressions have been used to model the spectral features of ambient noise since the days of Wenz (1962) and Piggott (1964). Carey and Fitzgerald (1993) presented a two-parameter logarithmic model which combined the wind speed dependence (n) and the spectral slope (m).

The characteristic features of measured ambient noise spectra are parametrized using a multi-parameter logarithmic model. The ambient noise spectrum level normalized to a 1-Hz band is approximated with a "frequency response" type curve fitted to the measurements. The noise model is made up of three segments (later referred to as "filter blocks") of different type and slope. The mathematical curve must be flexible enough to accurately follow the form of a measured ambient noise spectrum level. The expression for the ambient noise spectrum level may be written as

$$S(f) = S_0 + 10\log\left\{\frac{\left[1+\left(\frac{f_0}{f}\right)^{m_0}\right]}{\left[1+\left(\frac{f}{f_1}\right)^{m_1}\right]\left[1+\left(\frac{f_2}{f}\right)^{m_2}\right]}\right\}, \quad (6)$$

where S_0 is constant spectrum level; f_0, f_1, and f_2 are the critical (3 dB) frequencies of the filter blocks 0–2; and m_0, m_1, and m_2 are the spectral slope factors. A pure bandpass model is obtained using only the filter blocks 1 and 2. The

TABLE I. The model curve parameters used in Fig. 5.

Wind speed (m/s)	S_0 (dB//μPa/$\sqrt{}$Hz)	f_0 (Hz)	m_0	f_1 (Hz)	m_1	f_2 (Hz)	m_2
17	77	90	5.9	1500	1.9	180	4.0
7	66	130	6.6	1200	1.6	260	4.5
<3	49	230	3.2	2000	1.7	500	1
Calm	43	270	2.35	1000	1.20	⋯	⋯

model is illustrated in Fig. 3(a). The slopes of the blocks are obtained from the exponents m as

blocks 1 and 2: slope

$$= 10m_i \text{ dB/decade} \quad \text{or} \quad 3m_i \text{ dB/octave}, \quad i = 1,2,$$

block 0: slope

$$= 10(m_0 - m_2) \text{ dB/decade} \quad \text{or} \quad 3(m_0 - m_2) \text{ dB/octave}.$$

The bandwidth properties of ambient noise are studied using the effective noise bandwidth β_n (Burdic, 1991).

2. Wind speed dependence

The effect of the wind speed u on ambient noise level is studied with a four-parameter logarithmic expression capable of describing the wind speed dependence in three separate wind speed regions that represent different source mechanisms. The three-region model was introduced by Wilson (1983) and proposed again by Carey and Fitzgerald (1993). The first is a noise-limited region below the critical threshold wind speed u_c where no wave breaking occurs. The transition region starts from the onset of wave breaking at u_c. Above that the noise level rises with increasing wind speed at a rate determined by the wind speed dependence factor k. Above the saturation wind speed u_s is the high wind speed region where sea state conditions are fully developed and the noise level starts to saturate. The expression has similar elements to those in Eq. (6) and may be written as

$$S(u) = S_0 + 10 \log\left\{\frac{\left[1 + \left(\frac{u}{u_c}\right)^k\right]}{\left[1 + \left(\frac{u}{u_s}\right)^k\right]}\right\}, \tag{7}$$

where S_0 is the ambient noise spectrum level. Piggott (1964) studied the wind speed dependence of the noise intensity using the relationship $I \sim u^{2n}$. The wind speed dependence factor k in Eq. (7) is then twice Piggott's factor n; i.e., $n = k/2$. The model is illustrated in Fig. 3(b).

IV. RESULTS

The present data set comprises 44 uncontaminated ambient noise spectra covering the whole year. The wind speed ranges from calm to 17 m/s. The calm weather noise spectrum of unfrozen sea coincides with that measured under the ice cover in winter. All the 44 measured spectra are depicted in Fig. 4(a), which shows the overall range where the ambient noise spectrum level varies as a function of wind speed. In Fig. 4(b) the measured spectra are illustrated as a shaded surface which depicts the ambient noise in three dimensions as a function of frequency and wind speed. The gradual development of a low-frequency spectral decline below 300 Hz with increasing wind speed is clearly shown in the surface topography.

The spectra measured in the deep ocean have been shown to be fairly white below 500 Hz (Carey and Fitzgerald, 1993). Longuet-Higgins (1990) compiled and presented oceanic bubble noise spectra measured at shallow depths

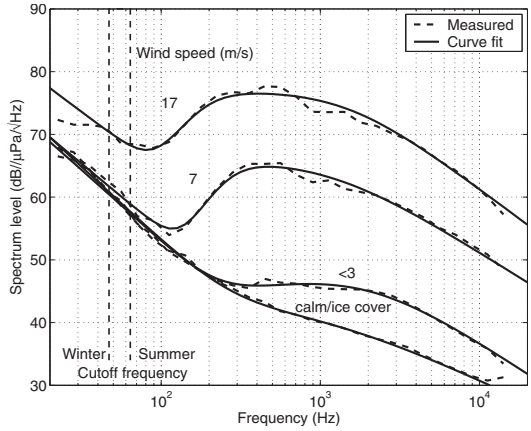

FIG. 5. Four model curves fitted to the measured noise spectra for the wind conditions of 17 m/s, 7 m/s, <3 m/s, and calm/ice cover. Cutoff frequencies for summer and winter conditions are depicted in the plot as vertical dashed lines.

(15–24 m) below a breaking wave which showed a spectral shape similar to that in present data. The low-frequency spectral decline in the FASINEX data originally measured by Farmer and Vagle (1989) was located roughly between 400 and 1000 Hz while in the present spectra the decline occurs between 100 and 300 Hz. The frequency shift may, at least partly, be attributed to the difference in salinity-controlled bubble size between the ocean and the archipelago water. Interestingly enough, the observed frequency ratio of 1 to 4 between the archipelago and ocean data seems to be the same that was predicted earlier from the bubble size measurements by Winkel *et al.* (2004).

The model curve of Eq. (6) was fitted to all of the spectra that yielded the set of seven parameters for each ambient noise spectrum. Figure 5 shows an example of fitting the curves to the measured noise spectra with four wind condition states, namely, calm, light, moderate, and high winds. The curves correspond closely with the steep depressions in 17 and 7 m/s spectra below 300 Hz. The curve fitting was mostly performed by a visual least-squares estimation where the parameters were manually adjusted to obtain the best fit. Numerical optimizing routines were also tried but the manual method provided the best control over the systematic behavior of the parameters. The model parameters for the fitted curves in Fig. 5 are compiled in Table I. In order to reveal possible cutoff effects in the measured spectra the cutoff frequency range (47–64 Hz) covering both summer and winter conditions is depicted in Fig. 5.

The ambient noise spectra show a bandpass shape where the maximum occurs between 400 and 600 Hz for wind speeds higher than 7 m/s. The absence of traffic noise reveals a sharp decline in ambient noise spectrum level below 300 Hz where the average spectral slope factor m_2 is about 3 (or 9 dB/octave) for medium wind speeds. This is nearly an order of magnitude higher than the m_2 value of $\sim 1/3$ (or 1 dB/octave) recorded from several diverse oceanographic areas (Carey and Fitzgerald, 1993) but very close to that iden-

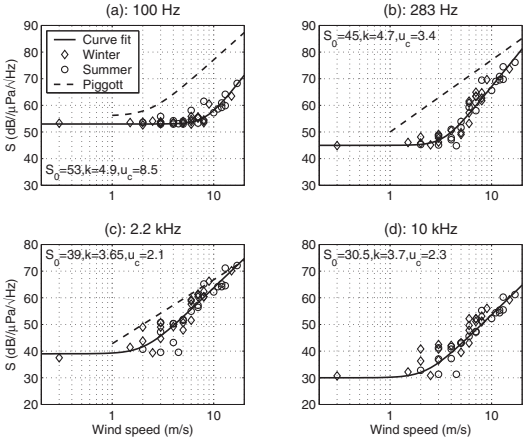

FIG. 6. Dependence of ambient noise on wind speed at 100 Hz (a), 283 Hz (b), 2.2 kHz (c), and 10 kHz (d). The curve fit parameters are also shown on the individual panels. The relationships reported by Piggott (1964) are depicted in the plots for comparison.

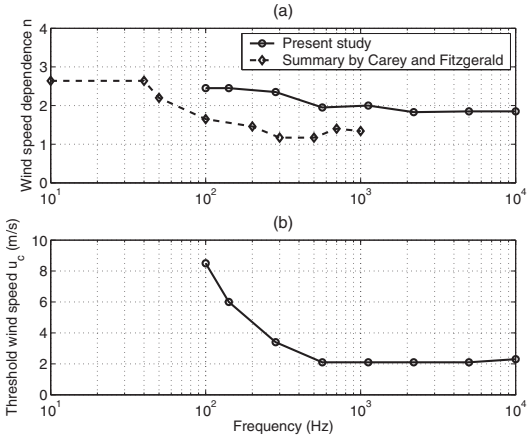

FIG. 7. (a) Wind speed dependence factors (n) compared to the earlier results. (b) Threshold wind speed versus frequency.

tified in the bubble noise spectra presented by Longuet-Higgins (1990). The shape of the spectrum also closely resembles that of the bubble spectrum by Franz (1959), which is illustrated by Ross (1987) together with the smoother impact spectrum. The spectral slope factor m_2 in the bubble spectra by Franz (1959) varies from 8 to 12 dB/octave in the $\frac{1}{2}$-octave band which corresponds to a slope factor of $m_2=5-9$ dB/octave in the 1-Hz band. The sharp decline is due to "the almost complete absence of bubbles larger than a certain size" (Franz, 1959; Wenz, 1962). The resonance frequency of 500 Hz for a single bubble corresponds to a bubble radius of 6.5 mm (Urick, 1983a) which is unrealistically large even for fresh water.

Theoretical calculations and experimental studies have demonstrated that the resonance frequencies of collective oscillations of bubble plumes and clouds are markedly lower than those of individual bubbles. In the tipping trough experiment that simulated a breaking wave event the observed resonance frequencies for a volume fraction of about 1% were around 100 Hz (Carey *et al.*, 1993). Yoon *et al.* (1991) concluded that a bubble cloud can radiate sound at frequencies substantially lower than the natural frequency of the individual bubbles and that most of the natural oceanic ambient noise below 1 kHz may be due to bubble clouds and plumes.

The wind speed dependence of the spectrum level at four frequencies between 100 Hz and 10 kHz are depicted in Fig. 6. The observations are divided into winter (diamond) and summer (circle) groups. The summer group contains the observations from May to mid-October while the winter group contains data collected during the rest of the year. The wind speed dependence factor k and the threshold wind speed u_c are obtained by fitting the model curve in Eq. (7) to the plots. The corresponding curves obtained by Piggott (1964) are shown together with the present results at frequencies from 100 Hz to 2.2 kHz. The spectrum levels have a distinctly increasing trend above the threshold wind speed u_c. No significant seasonal difference between the summer and winter observations is evident in the data.

Wind speed dependence factors ($n=k/2$) obtained from Fig. 6 are presented as a function of frequency in Fig. 7(a), together with the summary by Carey and Fitzgerald (1993). The dependence factors in the present study are systematically higher ($1.85<n<2.45$) than those in the summary data. Below 100 Hz the two curves seem to approach one another. Figure 7(b) shows how the threshold wind speed (u_c) decreases with increasing frequency, leveling off to a value of 2 m/s (~4 kn) at frequencies above 500 Hz.

Maximum spectrum levels above 100 Hz are typically located in the frequency range 400–1000 Hz, depending on wind speed. Figure 8(a) shows the maximum spectrum level ($S_{\max}$) as a function of wind speed. The three-region model in Eq. (7) was fitted to the maximum levels. The best fit was obtained with the following parameters: threshold wind speed $u_c=3.5$ m/s, wind speed dependence factor $k=5.3$

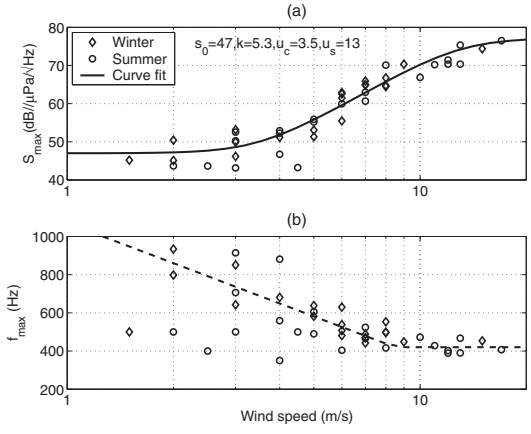

FIG. 8. (a) Maximum spectrum levels of ambient noise versus wind speed and (b) the corresponding frequencies. The model curve is fitted to the maximum level data.

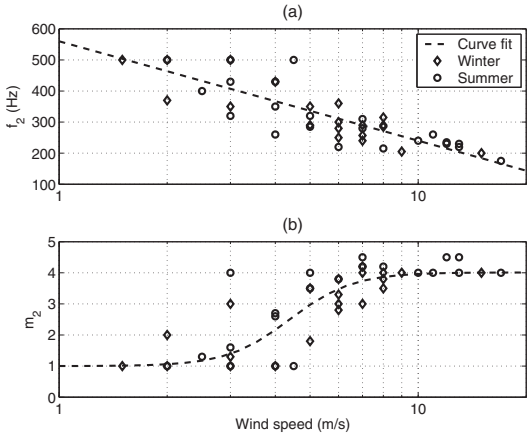

FIG. 9. Highpass filter parameters versus wind speed: critical frequency f_2 in (a) and spectral slope m_2 in (b).

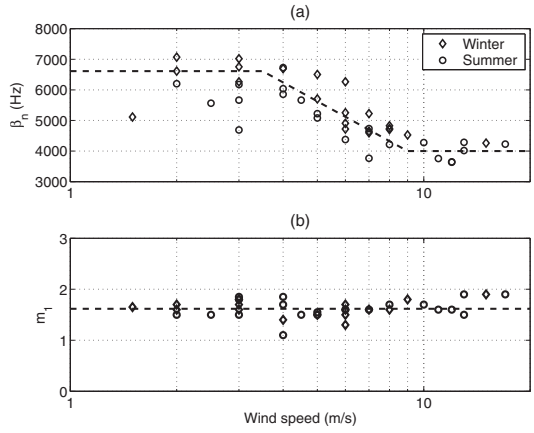

FIG. 10. (a) Noise bandwidth as a function of wind speed. The three-segment dashed line separates stable and changing parts from one another. (b) High-frequency spectral slope m_1 versus wind speed. The dashed line indicates the average slope of −4.9 dB/octave.

(n=2.65), and saturation wind speed u_s=13 m/s. Figure 8(b) shows how the position of the maximum shifts from ~900 Hz down to 400 Hz as the wind speed increases. This could mean that the average bubble size in breaking waves tends to grow with increasing wind speed. The deviation of the frequency values is large at lower wind speeds but it decreases markedly as wind speed increases. This may indicate that a dominating maximum bubble size is reached at wind speeds around 10 m/s.

The band limited structure of the ambient noise spectrum reflects the bubble size distribution in breaking waves. Suitable model parameters for describing the bandpass features of the spectrum are the highpass critical frequency f_2, the corresponding slope factor m_2, and the noise bandwidth β_n. Figure 9(a) shows the frequency f_2 as a function of wind speed. The corresponding spectral slope factor m_2 is depicted in Fig. 9(b). The critical frequency f_2 marks the start of the descending part of the spectrum below the broad maximum and shows a clear tendency to decrease as wind speed increases. At gale force winds f_2 falls below 200 Hz. This probably reflects the growth of the maximum bubble size with increasing wind speed, as observed in Fig. 8(b). The spectral slope factor m_2 in Fig. 9(b) increases as wind speed increases and reaches a saturation level of m_2=~4 (or 12 dB/octave) around 10 m/s. The noise bandwidths of the spectrum levels are depicted in Fig. 10(a). At light winds the noise bandwidth is larger and has a greater deviation. As wind speed increases above 10 m/s the noise bandwidth gets narrower until it levels off at a value of ~4 kHz. This exhibits a similar pattern to that observed in $f_{\max}$ [Fig. 8(b)] and in m_2 [Fig. 9(b)]. The threshold wind speed at 3–4 m/s probably indicates the onset of wave breaking and the saturation of the bandwidth again seems to begin at wind speeds of 8–10 m/s.

The high-frequency spectral slope factor m_1 remains fairly constant at all wind speeds, the average being −4.9 dB/octave, Fig. 10(b). This is slightly less than the typical values for deep water slopes of ~−6 dB/octave (Kerman, 1984).

V. COMPARISONS AND DISCUSSION

The ambient noise spectra obtained during the present study are compared to the results from the earlier studies. The average deep water spectra compiled by Urick (1983b) are plotted together with the present spectra corresponding to the same wind speeds, Fig. 11 (see the parameters in Table II). The maximum spectrum levels in the highest wind speed class are the same to within a few decibels but the wind speed dependences differ markedly from each other, as already demonstrated in Fig. 7(a), which shows $n(200)$~1.5 for deep ocean ambient noise and $n(200)$~2.4 for the present shallow water noise. The present spectra have a sharp decline below 500 Hz, giving them a shape characteristic of

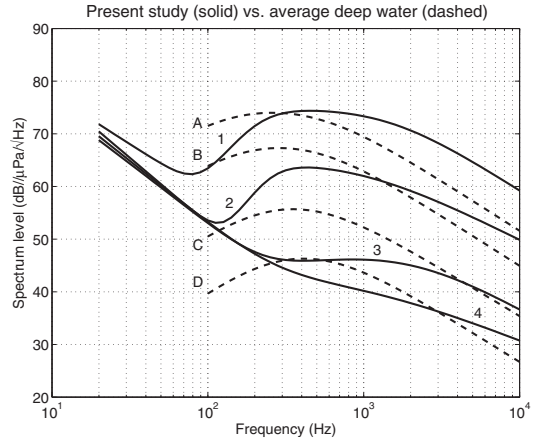

FIG. 11. Ambient noise curves of the present study (solid lines) compared to the average deep water curves (dashed lines). The present curves are marked with numbers denoting the wind speeds 14–16 m/s (1), 6–8 m/s (2), <3 m/s (3), and calm/ice cover (4). The deep water curves are marked in capitals as SS 6: 14–16 m/s (a), SS3: 5–8 m/s (b), SS1: <3 m/s (c), and SS0: <0.5 m/s (d).

TABLE II. The model curve parameters used in Fig. 11.

Wind speed (m/s)	S_0 (dB//μPa/$\sqrt{}$Hz)	f_0 (Hz)	m_0	f_1 (Hz)	m_1	f_2 (Hz)	m_2
			Present study				
14–16	75	87	5.9	1500	1.9	210	4.0
6–8	65	125	7.3	1000	1.5	250	4.8
<3	49	230	3.2	2000	1.7	500	1
Calm	43	270	2.35	1000	1.2	⋯	⋯
			Deep water				
14–16 (SS 6)	76	⋯	⋯	520	1.9	130	2
5–8 (SS 3)	70	⋯	⋯	480	1.9	170	2
2–3 (SS 1)	60	⋯	⋯	430	1.8	270	2
<0.5 (SS 0)	50	⋯	⋯	550	1.85	290	2.1

bubble type spectra while the deep water spectra are more reminiscent of the impact type (Franz, 1959; Longuet-Higgins, 1990; Ross, 1987). One of the reasons for this is the total absence of traffic noise in the present data, which enables recognition of wind-generated spectral features at lower frequencies. Another reason may be poor vibration isolation at lower frequencies in some suspended hydrophone systems. Strong tidal currents in ocean environments may cause mechanical vibrations in hydrophone structures which in turn raise low-frequency ambient noise. The hydrophone in this study was rigidly mounted on the sea bed and the tidal currents are negligible throughout the whole Baltic Sea basin. Other possible explanations could be differences between breaking waves in the ocean and archipelago environments. Bubble sizes and their distributions differ from each other due to the marked salinity difference. In an ocean environment wind speeds of 14–16 m/s develop a sea state 6 where significant wave height is 4–6 m. The corresponding significant wave height for the present brackish water archipelago environment is only 0.5–1 m. This means that the breaking waves in both environments must be quite different in structure and dynamics. It seems that in the confined archipelago waters the role of oscillating bubble clouds and plumes may dominate over impact sources in sound generation, thus emphasizing the resonance type features in the ambient noise spectrum below 500 Hz.

For frequencies greater than the local maximum the spectral slope for the present shallow water data is about 1 dB/octave less than that in the ocean environment. This may be attributed to differences in bubble size distribution and sound generating mechanisms between the breaking waves in the archipelago and ocean environment. No significant seasonal effects are found in the parameters calculated from the full 1-year data set.

VI. CONCLUSION

The present shallow water ambient noise measurements were carried out in a brackish water environment where the depth of the hydrophone was 15 m. The measurement site was well isolated from traffic noise which made it possible to study wind-generated effects at lower frequencies. Due to the near field conditions the ambient noise levels were not significantly distorted by propagation effects. The ambient noise spectrum levels develop a bubble type bandpass structure above 100 Hz as the wind speed increases. The observed sharp spectral declines below 500 Hz are most likely caused by the resonances of oscillating bubble clouds created by breaking waves. The low frequency range of the declines may be attributed to the larger bubble sizes in fresh and brackish waters.

The ambient noise levels are in fairly good agreement with the average deep water levels for the highest wind speeds but the wind speed dependences differ markedly from each other. In shallow brackish water the wind speed dependence factor at 200 Hz is ~2.4 which is significantly higher than the typical factor of ~1.5 for the ocean environment. The observed high-frequency spectral slope $m_1 \sim -5$ dB/octave remains fairly constant at all wind speeds but is about 1 dB/octave less than the typical deep water slope of ~−6 dB/octave. The measurements were carried out in all four seasons of the year but no significant seasonal effects were found in any parameter calculated from the spectra. The preferred explanation for the different spectral characteristics observed in the present data is that the bubble size distribution and sound generating mechanisms in breaking waves differ in the archipelago and ocean environment.

ACKNOWLEDGMENTS

This work was funded by the Finnish Naval Research Institute (FNRI). The authors would like to thank Mr. Pekka Kannari and Dr. Martti Kalliomäki for encouraging attitude during the course of the work and many useful discussions and comments on the manuscript, and Mr. Harri Vähätalo and Mr. Reino Riuttula for assisting in setting up and calibrating the hydrophone systems.

Burdic, W. S. (**1991**). *Underwater Acoustic System Analysis* (Prentice-Hall, Englewood Cliffs, NJ), pp. 429–433.

Burgess, A. S., and Kewley, D. J. (**1983**). "Wind-generated surface noise source levels in deep water east of Australia," J. Acoust. Soc. Am. **73**, 201–210.

Carey, W. M., and Browning, D. (**1988**). "Low frequency ocean ambient noise: Measurements and theory," in *Natural Mechanisms of Surface Generated Noise in the Ocean*, edited by B. R. Kerman (Kluwer, Dordrecht, The Netherlands), pp. 361–376.

Carey, W. M., and Fitzgerald, J. W. (**1993**). "Low frequency noise from breaking waves," in *Sea Surface Sound (2): Natural Physical Sources of Underwater Sound*, edited by B. R. Kerman (Kluwer, Dordrecht, The

Netherlands), pp. 277–304.
Carey, W. M., Fitzgerald, J. W., Monahan, E. C., and Wang, Q. (**1993**). "Measurement of the sound produced by a tipping trough with fresh and salt water," J. Acoust. Soc. Am. **93**, 3178–3192.
Farmer, D. M., and Vagle, S. (**1989**). "Waveguide propagation of ambient sound in the ocean-surface bubble layer," J. Acoust. Soc. Am. **86**, 1897–1908.
Franz, G. J. (**1959**). "Splashes as sources of sound in liquids," J. Acoust. Soc. Am. **31**, 1080–1096.
Ingenito, F., and Wolf, S. N. (**1989**). "Site dependence of wind-dominated ambient noise in shallow water," J. Acoust. Soc. Am. **85**, 141–145.
Jensen, F. B., Kuperman, W. A., Porter, M. B., and Schmidt, H. (**1994**). *Computational Ocean Acoustics* (American Institute of Physics, Woodbury, NY), pp. 28–33.
Kennedy, R. M., and Szlyk, T. K. (**1991**). "Modeling high-frequency vertical directional spectra," J. Acoust. Soc. Am. **89**, 673–681.
Kerman, B. R. (**1984**). "Underwater sound generation by breaking wind waves," J. Acoust. Soc. Am. **75**, 149–165.
Kullenberg, G. (**1981**). "Physical oceanography," in *The Baltic Sea*, Elsevier Oceanography Series Vol. **30**, edited by A. Voipio (Elsevier, Amsterdam, The Netherlands), pp. 135–181.
Kuperman, W. A., and Ferla, M. C. (**1985**). "A shallow water experiment to determine the source spectrum level of wind generated noise," J. Acoust. Soc. Am. **77**, 2067–2073.
Longuet-Higgins, M. S. (**1990**). "Bubble noise spectra," J. Acoust. Soc. Am. **87**, 652–661.
Lurton, X. (**2002**). *An Introduction to Underwater Acoustics* (Springer/Praxis, Chichester, UK), pp. 103–122.
Piggott, C. L. (**1964**). "Ambient sea noise at low frequencies in shallow water of the Scotian Shelf," J. Acoust. Soc. Am. **36**, 2152–2163.
Poikonen, A., and Madekivi, S. (**2005**). "Recent hydroacoustic measurements and studies in the Gulf of Finland," in *Proceedings of the 1st International Conference on Underwater Acoustic Measurements: Technologies and Results*, edited by J. S. Papadakis and L. Bjørnø (IACM-FORTH, Heraklion, Greece).
Prosperetti, A. (**1988**). "Bubble-related ambient noise in the ocean," J. Acoust. Soc. Am. **84**, 1042–1054.
Ross, D. (**1987**). *Mechanics of Underwater Sound* (Peninsula, Los Altos, CA), pp. 70–71.
Su, M.-Y., and Cartmill, J. (**1995**). "Effects of salinity on breaking wave generated void fraction and bubble size spectra," in *Proceedings of Air-Water Gas Transfer*, edited by B. Jähne and E. Mohanan (AEON, Hanau, Germany), pp. 305–311.
Urick, R. J. (**1983a**). *Principles of Underwater Sound* (Peninsula, Los Altos, CA), pp. 251–252.
Urick, R. J. (**1983b**). *Principles of Underwater Sound* (Peninsula, Los Altos, CA), pp. 210–211.
Urick, R. J. (**1984**). *Ambient Noise in the Sea* (Peninsula, Los Altos, CA).
Wenz, G. M. (**1962**). "Acoustic ambient noise in the ocean: Spectra and sources," J. Acoust. Soc. Am. **34**, 1936–1956.
Wilson, J. H. (**1983**). "Wind-generated noise modeling," J. Acoust. Soc. Am. **73**, 211–216.
Winkel, E. S., Ceccio, S. L., Dowling, D. R., and Perlin, M. (**2004**). "Bubble-size distributions produced by wall injection of air into flowing freshwater, saltwater and surfactant solutions," Exp. Fluids **37**, 802–810.
Yoon, S. W., Crum, L. A., Prosperetti, A., and Lu, Q. (**1991**). "An investigation of the collective oscillations of a bubble cloud," J. Acoust. Soc. Am. **89**, 700–706.